

Stamping Foreign Objects Monitoring Using Vibro-Acoustic Signal Morphological Differences

Runhui Long, Runye Lu, and Yanfeng Shen*

University of Michigan-Shanghai Jiao Tong University Joint Institute, Shanghai Jiao Tong University,
Shanghai, 200240, China

ABSTRACT

Stamping, a fundamental manufacturing process, is extensively employed across diverse industries, including automotive, aerospace, electronics, etc. Given the massive demand for efficient stamping processes, product quality control has become increasingly imperative. A critical challenge lies in the presence of foreign objects which can compromise product quality and machine integrity. Traditional manual inspection methods are labor-intensive, time-consuming, and costly, necessitating advanced condition monitoring techniques. This article introduces a real-time monitoring method for foreign objects detection during stamping processes. This method leverages vibro-acoustic signals captured by piezoelectric sensors, and employs mutual information comparison algorithms to evaluate signal morphological differences for anomaly detection. Validations of the method were conducted on both a laboratory press and a 200-ton industrial mechanical press. In laboratory settings, the method successfully detected foreign objects with a minimum area of 0.5 mm^2 at zero false positive rates, demonstrating exceptional accuracy. In practical industrial scenarios, it achieved a false positive rate of less than 10% for detecting foreign objects as small as 1 mm^2 . These results demonstrated the method's capability to enhance product quality of stamping parts and minimize material waste through early anomalies detection. This research provides a promising solution for anomalies detection in stamping process, empowering intelligent manufacturing.

Keyword: stamping; foreign objects detection; piezoelectric sensors; vibro-acoustic signals; mutual information; online condition monitoring

1 INTRODUCTION

Stamping is a fundamental manufacturing process widely employed in the fabrication of components for various manufacturing industries, including automotive, aerospace, electronics, home appliances, etc. [1]. This process utilizes dies and punches to shape metal into specific forms with high precision and accuracy [2]. However, one of the critical challenges faced during stamping operations is the occurrence of foreign objects such as metal debris within the production environment, which can lead to defects on the stamped parts and damage to the expensive tooling used in the process [3]. These consequences necessitate real-time condition monitoring for detecting foreign objects during stamping processes.

The traditional anomaly monitoring methods were conducted by manually inspecting the products being manufactured, arising challenges such as low inspection efficiency and delay

*Corresponding author:

E-mail address: yanfeng.shen@sjtu.edu.cn

in the detection of abnormalities [3, 4]. In recent years, many researchers have investigated different approaches to monitor the stamping process, encompassing strain measurement, force measurement, mutual inductance-based techniques, servo motor torque measurement, machine vision, acoustic emission, vibration-based methodologies, etc. Strain-based methods were achieved by employing autoregressive models [5], empirical mode decomposition (EMD) [6, 7], and wavelet transforms [7] to extract signal features, computing indicators like Hilbert marginal spectrum [6], and applying Hidden Markov Models (HMM) [5] or learning vector quantization (LVQ) [6] to classify faulty conditions including mis-feed, material thickness, etc. Regarding the force-based methods, recurrence quantification analysis (RQA) [8, 9], principal component analysis (PCA) [10, 11], and Haar transform [12], etc., were utilized to process signal and extract signal features, while different approaches such as regression analyses [11], a two-step control chart strategy [12], and a self-learning parameter selection (SLPS) algorithm [9] were developed for fault detection, achieving monitoring of forming defects like wrinkles and fractures [8], tool conditions like wear progression and lubrication states [10, 13], etc. Moreover, sensor fusion encompassing global and local force sensors, acoustic sensors, and strain gauges was achieved by a data lake, and correlation analysis was utilized to predict tool health and prevent failures [14]. Regarding the mutual inductance-based techniques, they were employed to track the local draw-in amount of sheet metals, by analyzing the induced electromotive force [15]. Furthermore, the servo motor torque measurement aimed at punch and die failure detection, by analyzing the servo motor torque of servo press machine and the punch time [16]. Although these studies investigated various sensing techniques to monitor several kinds of anomalies during stamping processes, few studies focused on the monitoring of anomaly caused by foreign objects.

Machine vision-based methods employed industrial cameras to detect foreign objects in stamping environment or surface defects on the workpiece through image analysis techniques. Approaches such as a Shape- and Size-Adaptive Descriptor (SSAD), a valley-emphasis Otsu method, and percolation-based shape recognition were utilized to extract shape and size features of the captured object [1, 3], while machine learning (ML) methods like a Local and Global Self-Supervised (LGSS) network were used to detect surface defects [4]. Moreover, an improved unsupervised homography estimation model was developed to enhance accuracy in aligning template images with target images [17], and a multi-angle illumination strategy were combined with plane illumination to locate and segment parts according to gray anomaly and highlight tiny defects [18]. However, these methods are inherently limited to monitoring regions within the camera's field of view, restricting their applicability in complex tooling environments with occlusions or multi-layered dies.

Among state-of-the-art methodologies, more relevant anomaly monitoring methods based on acoustic emission (AE) techniques were achieved by leveraging different signal features as indicators and algorithms to identify correlations between these features and anomalies. To be specific, signal features encompassing time-domain signal characteristics [19-21], spectral properties [22-24], energy content [23, 25, 26], etc., were employed, and anomaly detection

algorithms such as a time-domain amplitude ratio algorithm [21] and a Hilbert-Huang transform (HHT)-based mean frequency estimate algorithm [24] were developed. Tool anomalies including tool wear [20, 24, 26, 27], tool size [20], and lack of lubrication [26], material anomalies like stock thickness [20], and workpiece anomalies like cracking [21] were investigated. Furthermore, ML was employed on HHT-enhanced AE signals, by combining supervised learning with unsupervised fuzzy clustering, achieving classification of galling wear states [27]. However, challenges remained in the monitoring of anomaly caused by foreign objects.

Regarding the vibration-based methods, accelerometers were used as sensors and specific signal features such as frequency band energy (FBE) [28], vibration amplitude in certain frequency ranges [29], etc., served as indicators for anomaly detection. Faulty conditions monitoring encompasses workpiece anomalies like thickness variations [28, 30] and misfeeding [28], tool failures like tool wear [29, 31] and punch breakage [29, 32], etc. Approaches such as logistic regression models [32] and an adaptive 1D convolutional neural network [31] were utilized to evaluate tool wear conditions. Moreover, a diagonal-slice bispectrum algorithm was employed to suppress Gaussian noise and boost signal-to-noise ratio [30]. These studies showed the capability of using vibration signals in stamping anomaly monitoring. Nevertheless, limited research has been conducted on the foreign object detection. Ohashi [33] utilized the Mahalanobis-Taguchi system based on six extracted features from accelerometer signals to detect 30-mm-diameter floating scraps during stamping. However, challenges lay in high-precision anomaly monitoring towards foreign objects.

Addressing the limitations and deficiencies in the aforementioned methods, this study investigates an online monitoring method of stamping aiming at precisely detecting the foreign objects which would cause defects on the workpiece, by employing vibro-acoustic signals captured by piezoelectric sensors and mutual information-based algorithms to compare the morphological differences of signals. The developed method is capable of automatic foreign objects detection with high precision and real-time monitoring of stamping process, which not only enhances the product quality and reduces the loss caused by late detection, but also provides an intelligent solution of building lighthouse factories and achieving intelligent manufacturing.

This article commences with the introduction of the online monitoring method of stamping foreign objects, outlining the hardware and software frameworks, as well as the mutual information-based algorithms. Subsequently, the capability of the method is validated on a laboratory press, and the comprehensive algorithm proves to be effective for precise detection of foreign objects. Ultimately, an industrial test is implemented on a 200-ton mechanical press with different sizes of foreign objects, demonstrating the method's capability of achieving a high monitoring precision with a low false alarm rate. This article finishes with summaries, concluding remarks, and future work.

2 ONLINE MONITORING METHOD OF STAMPING FOREIGN OBJECTS

This section delineates the comprehensive architecture of the foreign objects online monitoring method, consisting of the hardware and software framework, as well as the mutual information comparison algorithm.

2.1 SENSOR DESIGN AND CHARACTERIZATION

The piezoelectric transducer (PZT) sensor assembly is specifically designed for integration into the stamping dies, as shown in Figure 1. The sensor assembly has dimensions of 42 mm × 21 mm × 7.1 mm, with the core of a PZT. Electrical connectivity is established through an RG178 coaxial cable terminated with an SMA interface connector, enabling a feasible connection to the data acquisition equipment. It is worth mentioning that a $39\text{ k}\Omega$ resistor is connected in parallel with the piezoelectric element to suppress DC offset drift through charge leakage path establishment. The sensing element was encapsulated in a custom aluminum housing, providing both electromagnetic shielding and mechanical protection. This compact encapsulation design enables direct embedment in stamping dies while maintaining structural integrity under dynamic loading conditions.

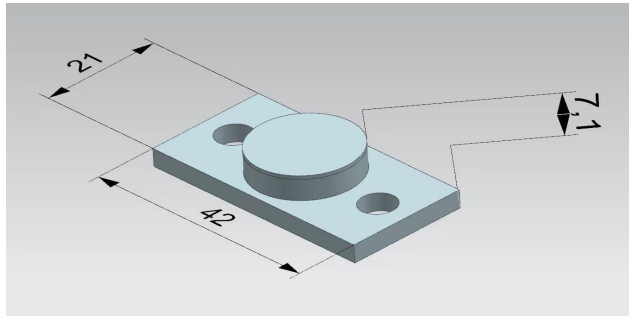


Figure 1: Piezoelectric transducer sensor.

2.2 DATA ACQUISITION HARDWARE DESIGN AND IMPLEMENTATION

The hardware framework of the system is composed of a punch press, a trigger unit, a piezoelectric sensing unit, data acquisition equipment (DAQ), an industrial PC, etc., as illustrated in Figure 2. Central to the system is the punch press, which is equipped with a trigger unit designed to synchronize the data acquisition process. The piezoelectric sensing unit comprises high-sensitivity PZT sensors bonded on the back surfaces of the upper and lower dies by adhesive. The back surfaces of the dies are machined with recesses corresponding to the dimensions of the sensors, and the sensors are adhered to the surface within these recesses using structural adhesive, forming intelligent dies. These sensors are responsible for capturing the vibro-acoustic signals during the stamping processes, and the acquired signals are relayed to the data acquisition system via coaxial cables equipped with SMA connectors. During each stamping cycle, the trigger unit can output a high-level voltage signal, which is subsequently transmitted to the DAQ equipment, synchronizing the active stamping process and data

acquisition. The vibro-acoustic signals are processed by the industrial PC and exploited for anomaly detection.

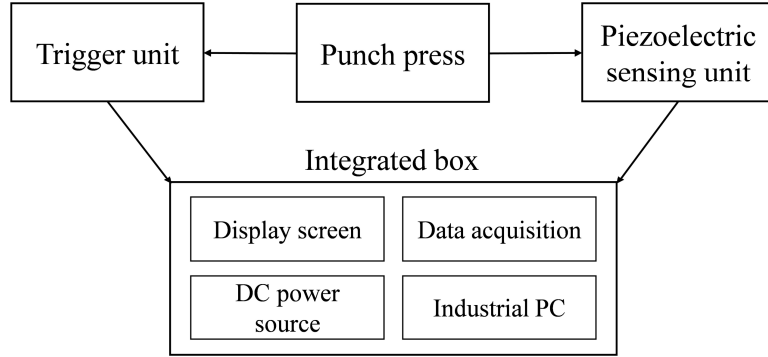


Figure 2: Hardware framework of online monitoring method of stamping foreign objects.

The practical configurations of the integrated box are displayed in Figure 3. The DAQ system is capable of handling 8 channels with a cumulative sampling frequency of 100 kHz, and is connected to the industrial PC through a USB port. The industrial PC is powered by an Intel Core i3 processor and a DC power source, serving as the computational hub for signal processing and anomaly detection. To facilitate user interaction, a touch-enabled display screen is mounted on the exterior of the integrated box, enabling real-time display and efficient user operations.

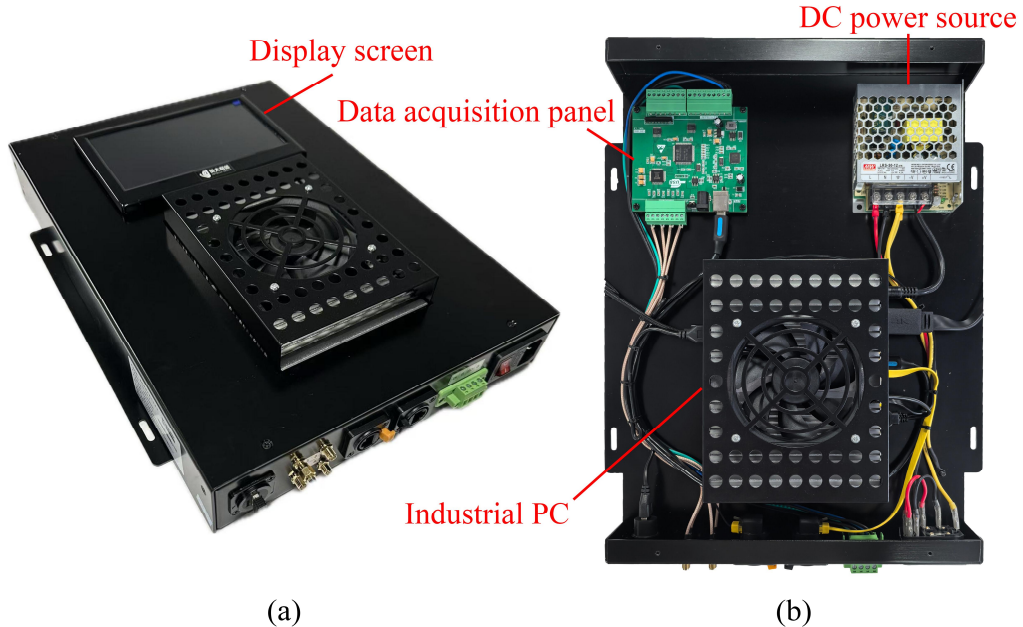


Figure 3: Practical configurations of integrated box: (a) exterior settings; (b) interior components.

2.3 GRAPHICAL USER INTERFACE

The software framework of the method is built on a Python-based platform, which achieves the interaction between hardware and software components and executes the core algorithms for data acquisition, processing, anomaly detection, and feedback control. A graphical user interface (GUI) developed using Qt Creator displays real-time signals, computation results, anomaly prediction outcomes, etc., as shown in Figure 4. On the left side of the interface, the channel selection module allows the user to choose a maximum of three different channels for DAQ, and the mode selection module allows three different modes which are “DAQ only” “DAQ & anomaly monitoring”, and “DAQ & anomaly monitoring & feedback control”. On the middle of the interface, the computation results of the selected channels of the current punch are updated in real time, as well as the anomaly prediction outcomes of each channel. On the right of the interface, the red and green indication bars can display the anomaly prediction outcomes of the last 30 punches. Furthermore, on the bottom of the interface, the processed signals of each selected channel of the current punch are displayed, and there is a module allows the adjustment of the system parameters such as the cut-off frequency, the threshold value, and so on, enabling the control of the monitoring accuracy of different channel sensors independently. The interface not only enables operators to monitor the stamping process with high efficiency, but also allows for the configuration of system parameters and the access of historical data, thereby facilitating comprehensive process analysis and optimization.

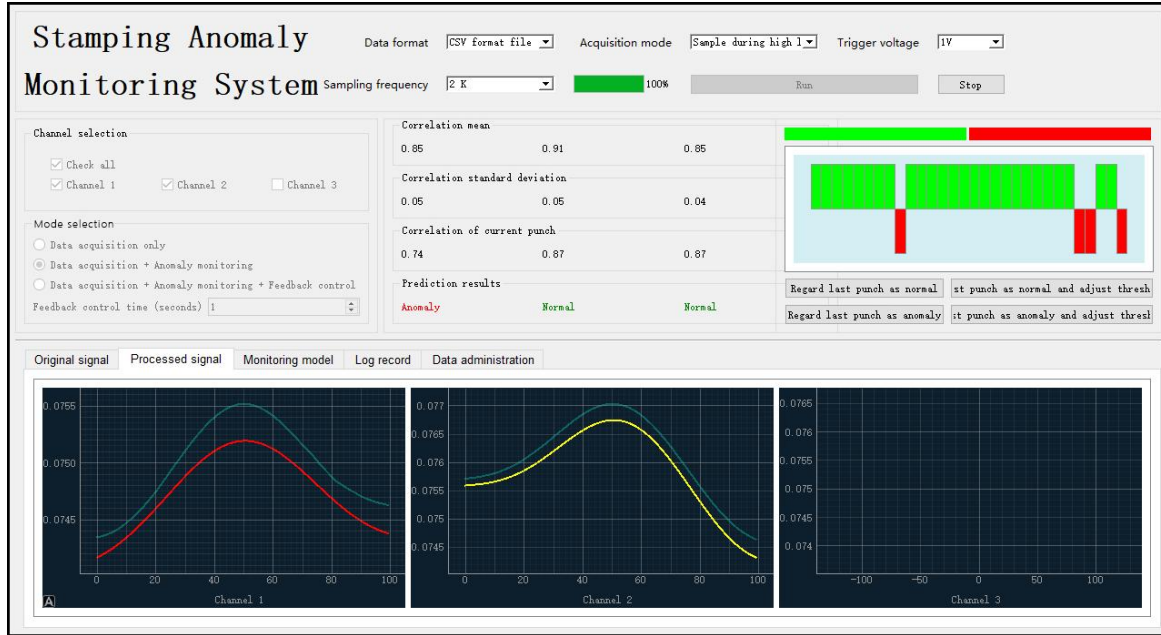


Figure 4: Graphical user interface of stamping anomaly monitoring system.

3 MUTUAL INFORMATION COMPARISON ALGORITHM

The core of the method lies in the mutual information comparison algorithm employed to evaluate signal morphological differences caused by foreign objects for anomaly detection.

3.1 SIGNAL PREPROCESSING

The algorithm commences with the processing on raw vibro-acoustic signals collected by the PZT sensors. A typical raw vibro-acoustic signal from a single pressing operation is shown in Figure 5 (a). To enhance signal clarity, a low-pass frequency filter is applied, and the processed signal is trimmed to isolate the section around the peak, as illustrated in Figure 5 (b).

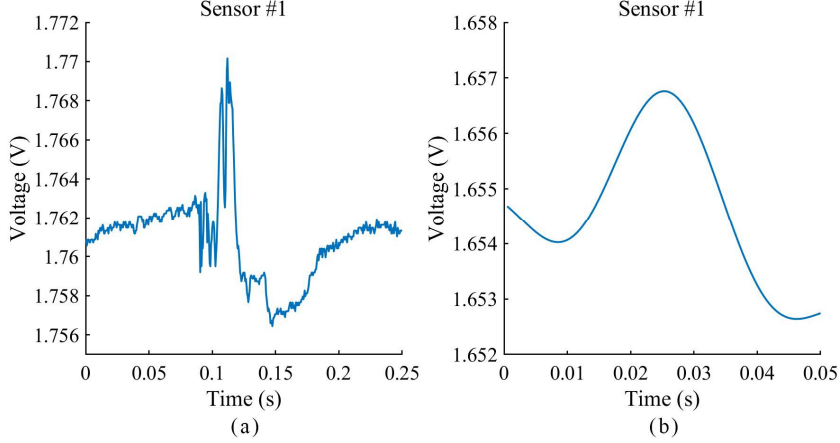


Figure 5: (a) Raw vibro-acoustic signal; (b) Processed signal.

After the abovementioned processing on the raw normal signals, a series of calibration signals are collected during multiple normal stamping cycles. The flow chart of the calibration process is depicted in Figure 6 (a). A baseline is established by computing the average of the calibration signals, serving as the reference for subsequent anomaly detection. The recommended number of calibration signals is 30, and the more calibration signals, the better accuracy of the baseline.

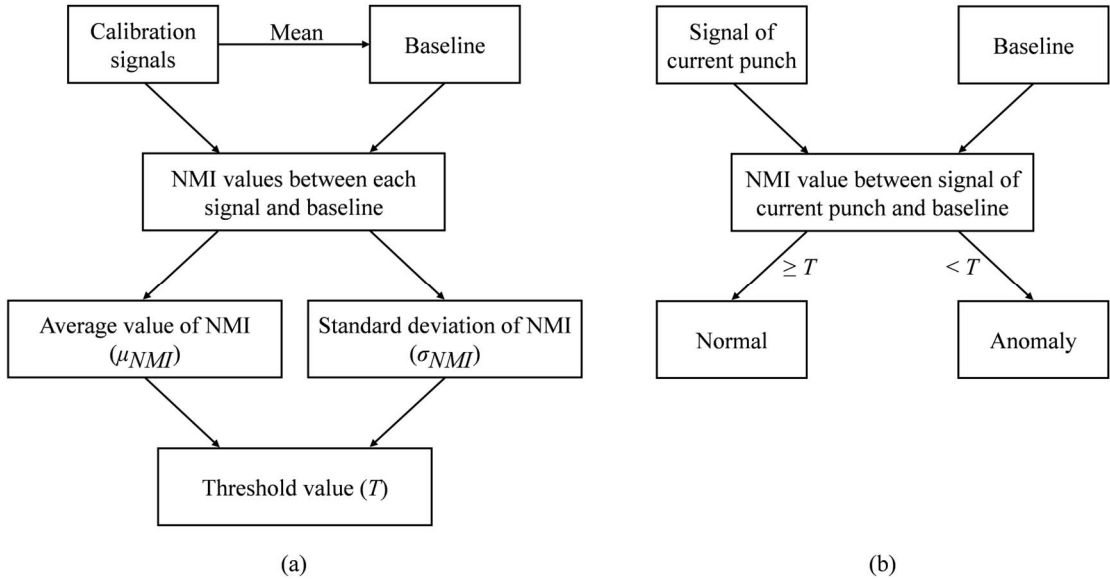


Figure 6: Flow chart: (a) calibration process; (b) prediction process.

3.2 NORMALIZED MUTUAL INFORMATION COMPUTATION

The normalized mutual information (NMI) between each calibration signal and the baseline signal is then calculated, the formulas of which are elucidated below. To compute mutual information, continuous signals must first be discretized. The number of bins is determined using Sturges' formula:

$$bins = 1 + \log_2 N,$$

where N is the length of the processed signals. The signal range is then divided into $bins$ equal intervals, mapping the value of each data point of the signal into an integer label to divide the signal range into $bins$ equal intervals, mapping each value to an integer label. For example, the signal values [0.1, 0.5, 0.9] might be discretized into [0, 1, 2]. This discretization approach adaptively determines the number of $bins$ based on data length N , balancing signal feature retention and computational efficiency.

After discretization, denote each discretized calibration signal and the discretized baseline signal as discrete variables X_{0i} ($i = 1, 2, 3, \dots$) and X_0 , respectively. The joint distribution of X_{0i} and X_0 is constructed, which is denoted as $p(x', x)$. The joint distribution represents the co-occurrence frequency of integer labels from both signals. For example, $p(1,1)$ represents the probability of $X_{0i} = 1$ and $X_0 = 1$. Marginal distributions of X_i and X_0 , denoted as $p(x')$ and $p(x)$, respectively, is obtained by summing the joint distribution over rows and columns:

$$p(x') = \sum_{x \in X_0} p(x', x), p(x) = \sum_{x' \in X_{0i}} p(x', x).$$

Mutual information $I(X_{0i}; X_0)$ is defined as:

$$I(X_{0i}; X_0) = \sum_{x' \in X_{0i}} \sum_{x \in X_0} p(x', x) \log \frac{p(x', x)}{p(x')p(x)}.$$

It quantifies the statistical dependence between X_i and X_0 , with higher values indicating stronger dependence. Information entropy measures the uncertainty of a random variable X and is defined as:

$$H(X) = -\sum_{x \in X} p(x) \log p(x),$$

where $p(x)$ is the probability that the random variable X takes x . High entropy indicates dispersed values, while low entropy implies concentration. To standardize mutual information into the range [0, 1], normalized mutual information can be calculated as:

$$NMI(X_{0i}; X_0) = \frac{2I(X_{0i}; X_0)}{H(X_{0i})+H(X_0)}.$$

The greater the NMI, the higher the dependency between two variables, as shown in Figure 7. $NMI(X_{0i}; X_0) = 1$ indicates perfect dependence, i.e. $X_{0i} = X_0$, while $NMI(X_{0i}; X_0) = 0$ means complete independence such as random noise. Normalization removes signal-specific uncertainty bias, enabling more accurate comparisons.

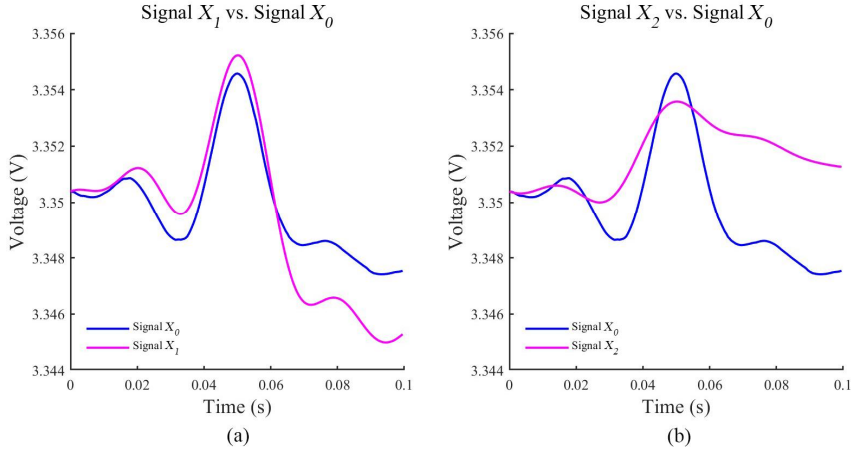


Figure 7: Comparison between two sets of typical signals: (a) high NMI; (b) low NMI.

3.3 PREDICTION OF FOREIGN OBJECT OCCURRENCE

The average value μ_{NMI} and standard deviation σ_{NMI} of the NMI values between each calibration signal and the baseline signal are computed to determine the threshold value T for anomaly detection, as described by the following equation:

$$T = \mu_{NMI} - k\sigma_{NMI},$$

where k is a specified multiple and is determined by the precision of foreign object detection, ensuring a balance between sensitivity and false alarm rate. At this stage, the calibration process is completed and the prediction of foreign objects is enabled. The flow chart of the prediction process is depicted in Figure 6 (b). The criterion for the occurrence of foreign objects is that, the NMI between the processed signal of current pressing operation and the baseline signal is lower than the threshold value T . By the mutual information comparison algorithm, the method can attain online foreign objects detection during stamping processes with high sensitivity.

4 EXPERIMENTAL IMPLEMENTATION ON LABORATORY PRESS

This section delineates the experimental implementation of the proposed method on a laboratory press. The system collaboration and the comprehensive algorithm are assessed under controlled conditions. Under the laboratory scenarios, the method achieves a zero false positive rate for detecting foreign objects as small as 0.5 mm^2 . This outcome underscores the method's reliability and validates its potential for practical application in precise stamping processes.

4.1 EXPERIMENTAL CONFIGURATIONS

The experimental configurations are demonstrated in Figure 8. An electric drive mechanical press with dimensions of $20 \text{ cm} \times 10 \text{ cm} \times 30 \text{ cm}$ is employed as a prototype press. The trigger unit is constructed using an NPN normally open laser through-beam photoelectric sensor, powered by a DC power supply delivering a 12V output. During each stamping cycle, a black

plastic sheet affixed to the crankshaft of the press blocks the laser beam due to the rotation of the crankshaft, causing the photoelectric sensor to output a high-level voltage signal during this period. This signal is transmitted to the data acquisition equipment, ensuring synchronization of data capture with the active stamping phase. Two piezoelectric sensors are bonded on the rear surfaces of the upper and lower dies, respectively. These sensors are connected to the integrated box through coaxial cables equipped with SMA connectors. Aluminum plates with dimensions of 100 mm*100 mm*3 mm are employed as prototype workpieces to simulate real-world stamping conditions.

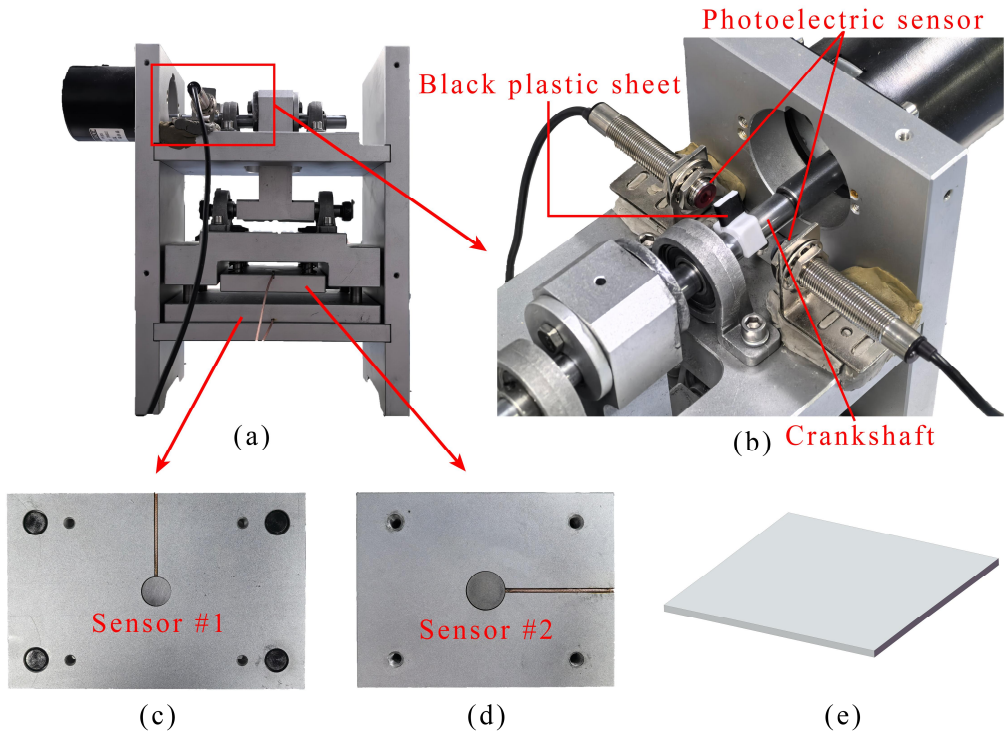


Figure 8: Experimental configurations: (a) laboratory press; (b) trigger unit; (c) sensor configuration of lower die; (d) sensor configuration of upper die; (e) aluminum plate workpiece.

4.2 FOREIGN OBJECTS DETECTION

The baseline for anomaly detection is established by computing the average of 30 signals acquired during normal stamping cycles. The NMI values between each signal and the baseline are calculated. For sensor #1 and sensor #2, the average NMI values are 0.686 and 0.709, respectively, with standard deviations of 0.0423 and 0.0525.

To evaluate the system's detection capability, three metallic scraps with an area of 0.5 mm², denoted as scrap 1, scrap 2, and scrap 3, are deliberately introduced between the workpiece and the lower die in three separate trials, as depicted in Figure 9. The processed vibro-acoustic signals of the three abnormal trials with scraps are plotted with the baseline, and the signal of

a typical normal trial is plotted for comparative analysis, as shown in Figure 10. The abnormal signals exhibit distinct morphological deviations from the baseline. For sensor #1, the signal peaks become blunted, and the decay rate diminishes. The scraps prolong the contact duration between the die and workpiece by introducing compliance or uneven surfaces, smoothing the sharpness of the signal peaks. Additionally, the energy dispersion caused by the scraps reduces the intensity of the initial impact, leading to the blunted peak morphology as well. As for the diminished decay rate, the presence of scraps in the die-workpiece interface increases system damping, by introducing frictional losses or localized plastic deformation, which slows the vibration decay. For sensor #2, the amplitude of the peaks decreases. Since sensor #2 is bonded on the rear of the upper die, the scraps act as barriers and dissipates part of the impact energy, making the effective force transmitted to the upper die and sensed by sensor #2 decrease, which results in the reduced amplitude of signal peaks. These signal morphological differences establish the foundation for anomaly detection based on NMI comparison.

	Scrap 1	Scrap 2	Scrap 3
Area	0.5 mm ²	0.5 mm ²	0.5 mm ²

Table 1: Dimensions of scraps in experimental implementation.

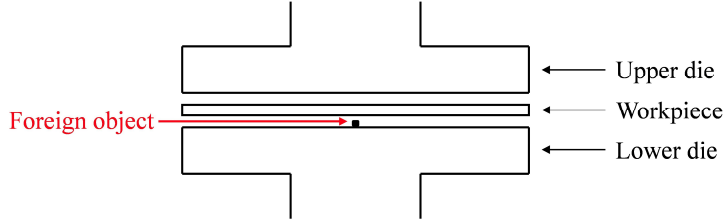


Figure 9: Schematic diagram of foreign objects placement in experimental implementation.

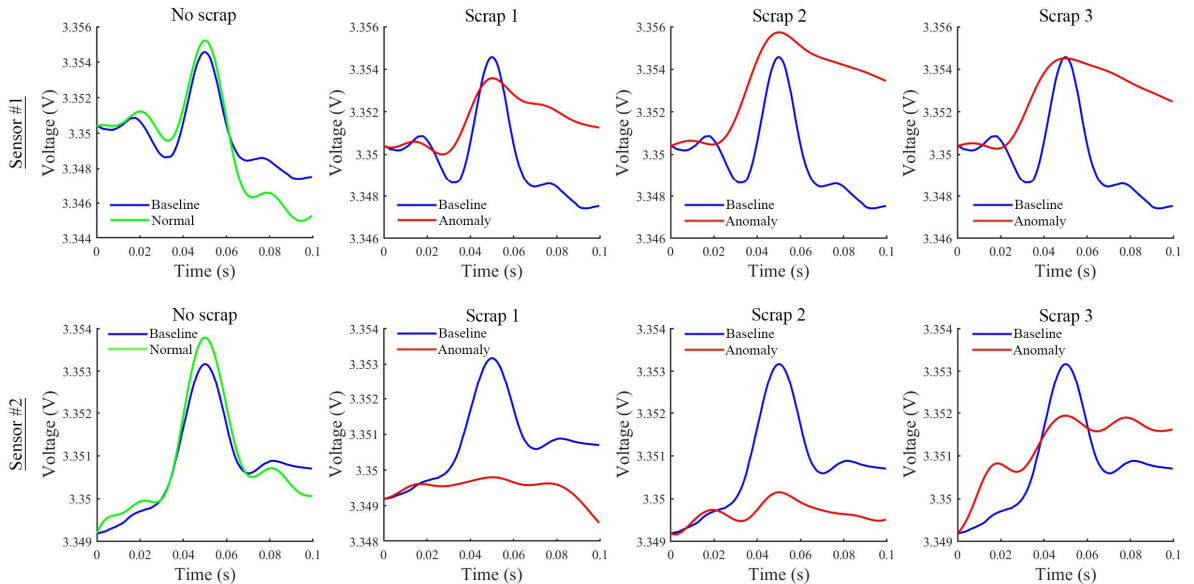


Figure 10: Signals of a normal trial and three abnormal trials for sensor #1 and sensor #2.

The NMI values between the abnormal signals and the baseline are computed and plotted alongside the normal values, as shown in Figure 11. A pronounced reduction in NMI values of the abnormal trials is observed for both sensors, resulting from the abovementioned signal morphological alterations caused by the presence of scraps. The threshold values for anomaly detection are set at the average NMI value minus three times the standard deviation, yielding threshold values of 0.559 for sensor #1 and 0.552 for sensor #2. Any trial whose NMI of sensor #1 is less than 0.559 or NMI of sensor #2 is less than 0.552 is classified as anomaly. In these settings, both sensors successfully detect all three scraps with zero false positive rates, demonstrating the method's high precision and stability to discern anomalies.

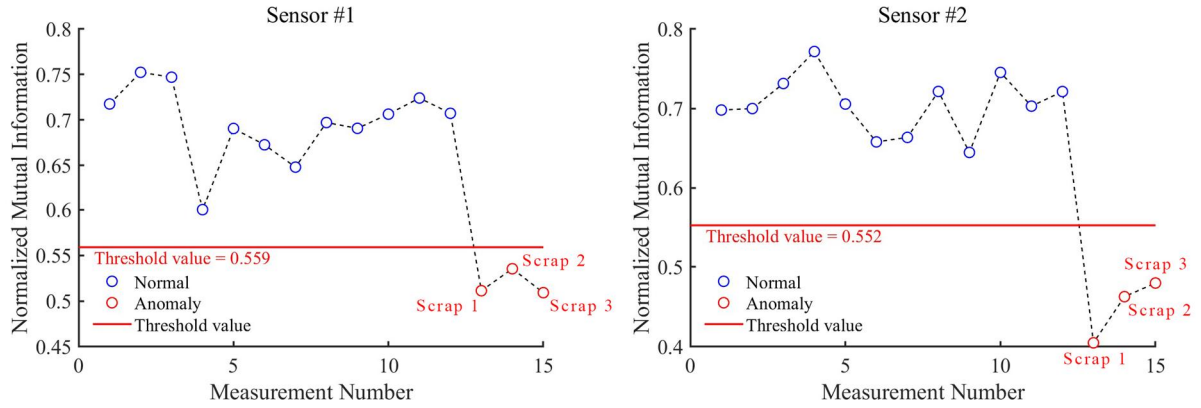


Figure 11: NMI values for sensor #1 and sensor #2.

	Sensor #1			Sensor #2		
μ_{NMI}	0.686			0.709		
σ_{NMI}	0.0423			0.0525		
k	3.0			3.0		
T	0.559			0.552		
	Scrap 1	Scrap 2	Scrap 3	Scrap 1	Scrap 2	Scrap 3
NMI	0.511	0.535	0.509	0.405	0.463	0.480

Table 2: NMI values for sensor #1 and sensor #2.

5 PRACTICAL DEMONSTRATION ON INDUSTRIAL PRESS

This section elucidates the practical implementation and validation of the proposed method on an industrial mechanical press, SEYI SN1-200 press, as shown in Figure 12(a). The demonstration is conducted in the I/O hole flanging process of manufacturing the backplane of an All-in-One PC shown in Figure 12(b), showcasing the method's capability of detecting foreign objects of varying sizes with high precision under real-world operating conditions.

5.1 CONFIGURATIONS OF PRACTICAL DEMONSTRATION

The industrial demonstration leverages the electronic cam of the SEYI SN1-200 press as the trigger unit. The electronic cam is configured to output a high-voltage signal during the crankshaft angle range of 165° to 195° , which corresponds to the active stamping phase. Four

piezoelectric sensors are bonded on the rear surfaces of the lower and upper dies, as illustrated in Figure 12(c) and (d), respectively. Sensor #1 is mounted on the stress-concentrated area of the lower die, while sensor #2, #3, and #4 are affixed to the upper die. It is worth mentioning that sensor #3 and #4 are not employed due to cause of force majeure.

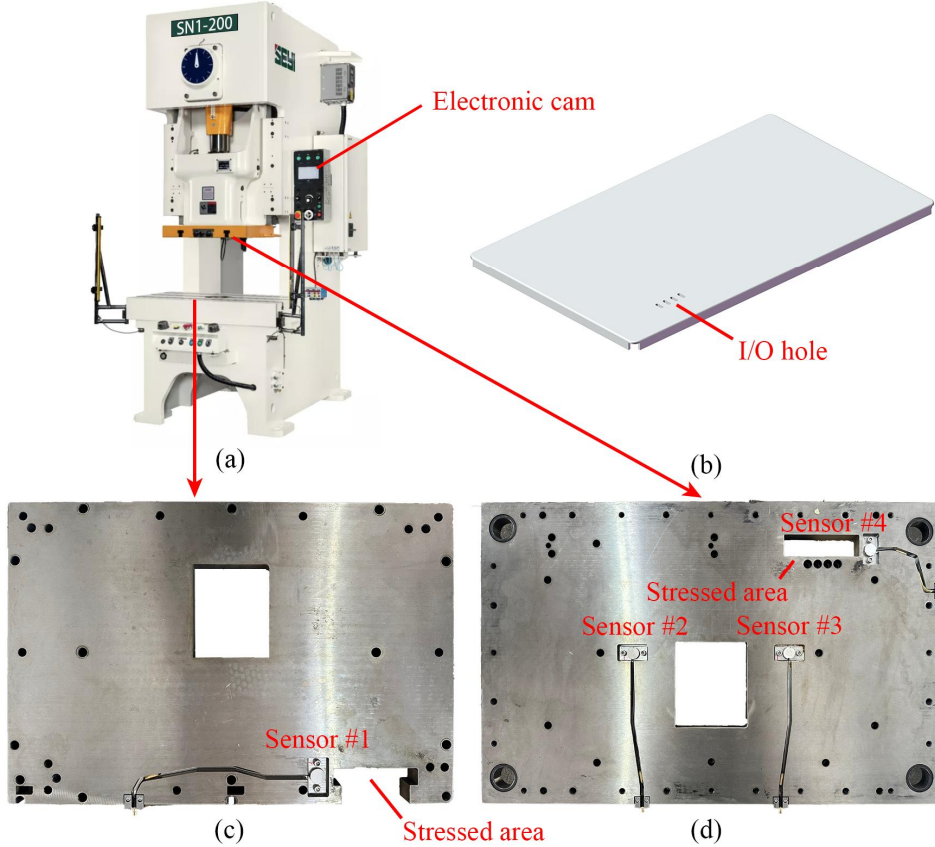


Figure 12: Practical configurations: (a) SEYI SN1-200 press; (b) backplane of an All-in-One PC; (c) sensor configuration of lower die; (d) sensor configuration of upper die.

5.2 FOREIGN OBJECTS DETECTION

A baseline for anomaly detection is established by averaging 82 normal vibro-acoustic signals acquired during consecutive stamping cycles. The NMI values between each calibration signal and the baseline are computed. For sensor #1 and sensor #2, the average NMI values are 0.854 and 0.918, respectively, with standard deviations of 0.0540 and 0.0536. Three metallic scraps that can cause defects with area of 5 mm^2 , 1.5 mm^2 , and 1 mm^2 , denoted as scrap 1, scrap 2, and scrap 3, respectively, are introduced beneath the stressed area of the workpiece in three separate trials, as depicted in Figure 13. The comparison of the processed signals from a typical normal trial and the three abnormal trials with scraps is shown in Figure 14. For abnormal signals of sensor #1, compared with the baseline, the signal peaks become sharper, and the decay rate increases. In industrial scenarios, the scraps made by iron is rigid and located near the force-bearing point where sensor #1 is placed, concentrating stress locally, which results in

more abrupt impact and generates sharper signal peaks. The more concentrated stress also leads to the faster signal decay, since the system dissipates energy more quickly after the more transient impact. In contrast, the abnormal signals from sensor #2 exhibit overall attenuation. This discrepancy is attributed to the greater distance between sensor #2 and the force-bearing point where the scraps are placed. The scraps placed beneath the workpiece act as barriers that disrupt direct force transmission to the upper die, reducing the effective energy sensed by sensor #2 and causing the overall attenuation of signals. It is worth mentioning that larger foreign objects such as scrap 1 may have two opposing effects on the vibro-acoustic signals captured by sensor #2. One is that the disruption of direct force transmission to the upper die makes the signal amplitude attenuate, while the other one is that the deformation of the large scrap during the stamping process produces additional vibration signals which increases the signal amplitude. The two opposite effects cancel each other out, which makes the resulting signal present no detectable changes, so that the system misidentifies the signal of sensor #2 from the trial with respect to scrap 1 as a normal signal.

	Scrap 1	Scrap 2	Scrap 3
Area	5 mm ²	1.5 mm ²	1 mm ²

Table 3: Dimensions of scraps in practical demonstration.

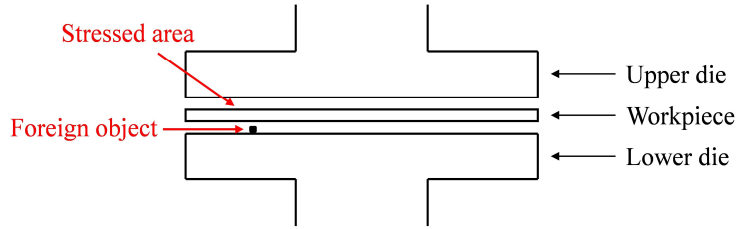


Figure 13: Schematic diagram of foreign objects placement in practical demonstration.

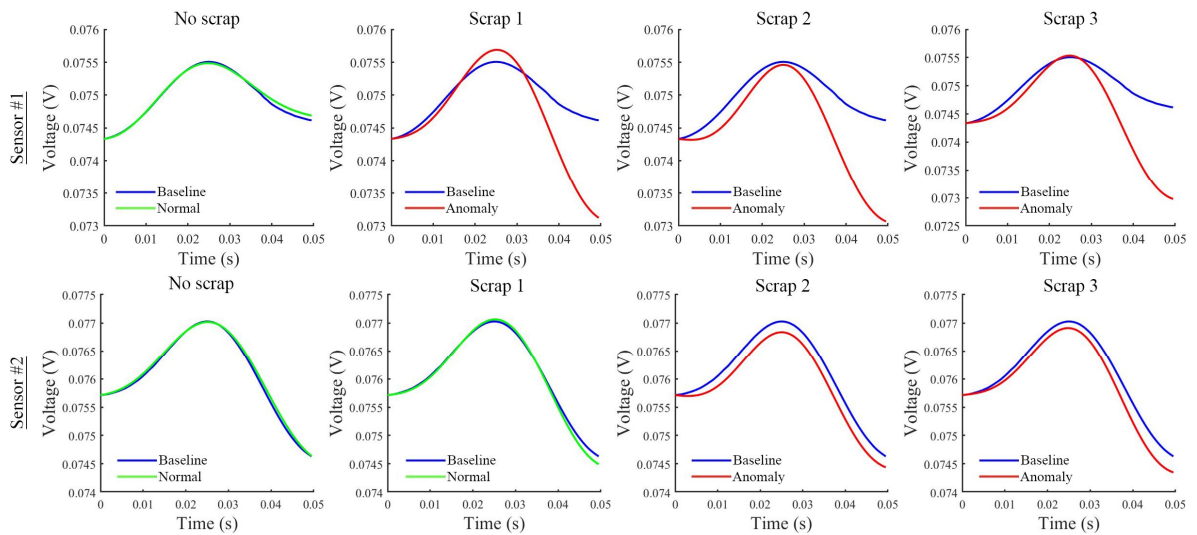


Figure 14: Signals of a normal trial and three abnormal trials for sensor #1 and sensor #2.

The NMI values between the resulting abnormal signals and the baseline are calculated and plotted alongside the normal values, as shown in Figure 15. A reduction in NMI values caused by the abovementioned morphological alterations is observed, indicating the presence of foreign objects. For sensor #1, all the scraps can be successfully detected by setting the threshold value to be the average value minus 1.5 times the standard deviation which equals to 0.773. For sensor #2, by setting the threshold value to be the average value minus 1.2 times the standard deviation which equals to 0.854, scrap 2 and scrap 3 can be detected while scrap 1 cannot be detected by the reasons mentioned earlier. The closer proximity of sensor #1 to the force-bearing area enhances its sensitivity to anomalies, underscoring the importance of sensor placement in optimizing detection accuracy. Under the current operational conditions, the system achieves a false positive rate of less than 10% for detecting foreign objects as small as 1mm^2 , further validating the method's ability to detect foreign objects with high precision and highlighting the method's reliability in industrial settings.

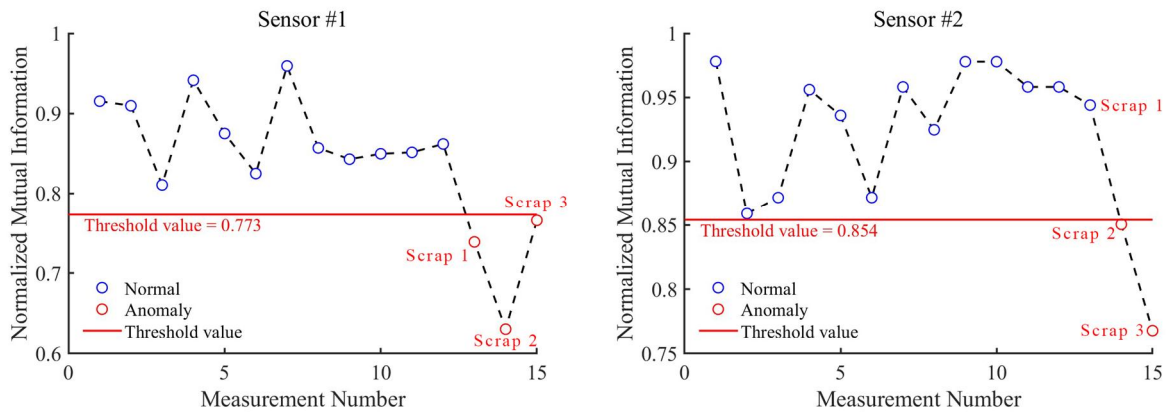


Figure 15: NMI values for sensor #1 and sensor #2.

	Sensor #1			Sensor #2		
μ_{NMI}	0.854			0.918		
σ_{NMI}	0.0540			0.0536		
k	1.5			1.2		
T	0.773			0.854		
	Scrap 1	Scrap 2	Scrap 3	Scrap 1	Scrap 2	Scrap 3
NMI	0.739	0.630	0.766	0.944	0.850	0.768

Table 4: NMI values for sensor #1 and sensor #2.

6 CONCLUSIONS AND FUTURE WORK

This study presents an innovative online monitoring method designed to detect foreign objects in stamping processes, leveraging vibro-acoustic signals captured by piezoelectric sensors and the morphological differences identified by the mutual information comparison algorithm. The method addresses the inefficiencies and limitations of traditional manual inspection methods by offering a real-time, automated solution for anomaly detection. The integration of the trigger unit, piezoelectric sensors, data acquisition equipment, the industrial PC, and the user-friendly

GUI, supported by a Python-based software framework, ensures robust condition monitoring. The method's efficacy is validated on both a laboratory press and an industrial SEYI SN1-200 press. In controlled laboratory conditions, the method demonstrated exceptional precision, achieving a zero false positive rate in detecting foreign objects as small as 0.5 mm^2 . Under real-world industrial operating conditions, the method achieves a false positive rate of less than 10% for detecting foreign objects as small as 1 mm^2 , further validating its reliability.

By enhancing product quality and reducing material waste, this method represents a significant step towards intelligent manufacturing. Its ability to provide precise, real-time stamping foreign objects detection offers a practical solution for industries reliant on high-precision stamping processes. Future work will focus on further optimizing sensor placement and algorithm parameter configurations to enhance detection sensitivity and reduce false positives, ensuring the system's adaptability to a broader range of industrial applications.

7 REFERENCES

- [1] Y. Miao, J. Y. Jeon, and G. Park, "An image processing-based crack detection technique for pressed panel products," *Journal of Manufacturing Systems*, vol. 57, pp. 287-297, 2020/10/01/ 2020, doi: 10.1016/j.jmsy.2020.10.004.
- [2] X. He, T. Welo, and J. Ma, "In-process monitoring strategies and methods in metal forming: A selective review," *Journal of Manufacturing Processes*, vol. 138, pp. 100-128, 2025/03/30/ 2025, doi: 10.1016/j.jmapro.2025.02.011.
- [3] L. Ma and F. Meng, "Anomaly Detection in the Production Process of Stamping Progressive Dies Using the Shape- and Size-Adaptive Descriptors," *Sensors*, vol. 23, no. 21, doi: 10.3390/s23218904.
- [4] X. Dong, C. Zhang, D. Wang, Q. Guo, X. Deng, and C. Li, "Inspection of cracking in stamping parts surfaces using anomaly detection," *Engineering Applications of Artificial Intelligence*, vol. 143, p. 110006, 2025/03/01/ 2025, doi: 10.1016/j.engappai.2025.110006.
- [5] M. Ge, R. Du, and Y. Xu, "Hidden Markov Model based fault diagnosis for stamping processes," *Mechanical Systems and Signal Processing*, vol. 18, no. 2, pp. 391-408, 2004/03/01/ 2004, doi: 10.1016/S0888-3270(03)00076-1.
- [6] A. M. Bassiuny, X. Li, and R. Du, "Fault diagnosis of stamping process based on empirical mode decomposition and learning vector quantization," *International Journal of Machine Tools and Manufacture*, vol. 47, no. 15, pp. 2298-2306, 2007/12/01/ 2007, doi: 10.1016/j.ijmachtools.2007.06.006.
- [7] X. Li and A. M. Bassiuny, "Transient dynamical analysis of strain signals in sheet metal stamping processes," *International Journal of Machine Tools and Manufacture*, vol. 48, no. 5, pp. 576-588, 2008/04/01/ 2008, doi: 10.1016/j.ijmachtools.2007.06.010.
- [8] I. Jang, G. Bae, and H. Kim, "Metal forming defect detection method based on recurrence quantification analysis of time-series load signal measured by real-time monitoring system with bolt-type piezoelectric sensor," *Mechanical Systems and Signal Processing*, vol. 180, p. 109457, 2022/11/15/ 2022, doi: 10.1016/j.ymssp.2022.109457.
- [9] C. Zhou, K. Liu, X. Zhang, W. Zhang, and J. Shi, "An Automatic Process Monitoring Method Using Recurrence Plot in Progressive Stamping Processes," *IEEE Transactions on Automation Science and Engineering*, vol. 13, no. 2, pp. 1102-1111, 2016, doi: 10.1109/TASE.2015.2468058.

- [10] B. M. Voss, M. P. Pereira, B. F. Rolfe, and M. C. Doolan, "Using stamping punch force variation for the identification of changes in lubrication and wear mechanism," *Journal of Physics: Conference Series*, vol. 896, no. 1, p. 012028, 2017/09/01 2017, doi: 10.1088/1742-6596/896/1/012028.
- [11] J. Jin and J. Shi, "Diagnostic Feature Extraction From Stamping Tonnage Signals Based on Design of Experiments," *Journal of Manufacturing Science and Engineering*, vol. 122, no. 2, pp. 360-369, 1999, doi: 10.1115/1.538926.
- [12] H. Shui, X. Jin, and J. Ni, "An Anomaly Detection and Diagnosis Method Based on Real-Time Health Monitoring for Progressive Stamping Processes," vol. 2, 06/08 2015, doi: 10.1115/MSEC20159420.
- [13] H. Kim, T. Altan, and Q. Yan, "Evaluation of stamping lubricants in forming advanced high strength steels (AHSS) using deep drawing and ironing tests," *Journal of Materials Processing Technology*, vol. 209, no. 8, pp. 4122-4133, 2009/04/21/ 2009, doi: 10.1016/j.jmatprotec.2008.10.007.
- [14] D. Farioli, E. Kaya, A. Fumagalli, P. Cattaneo, and M. Strano, "A Data-Based Tool Failure Prevention Approach in Progressive Die Stamping," *Journal of Manufacturing and Materials Processing*, vol. 7, no. 3, doi: 10.3390/jmmp7030092.
- [15] N. Mahayotsanun, S. Sah, J. Cao, M. Peshkin, R. X. Gao, and C.-t. Wang, "Tooling-integrated sensing systems for stamping process monitoring," *International Journal of Machine Tools and Manufacture*, vol. 49, no. 7, pp. 634-644, 2009/06/01/ 2009, doi: 10.1016/j.ijmachtools.2009.01.009.
- [16] L.-W. Chen and C.-T. Yeh, "Development of a real-time failure detection system for stamping die," *The International Journal of Advanced Manufacturing Technology*, vol. 120, no. 7, pp. 5623-5632, 2022/06/01 2022, doi: 10.1007/s00170-022-09055-w.
- [17] Y. Zhang and Y. Du, "Image Registration Algorithm for Stamping Process Monitoring Based on Improved Unsupervised Homography Estimation," *Applied Sciences*, vol. 14, no. 17, doi: 10.3390/app14177721.
- [18] H. Tian, D. Wang, J. Lin, Q. Chen, and Z. Liu, "Surface Defects Detection of Stamping and Grinding Flat Parts Based on Machine Vision," *Sensors*, vol. 20, p. 4531, 08/13 2020, doi: 10.3390/s20164531.
- [19] B. S. Kim, "Punch Press Monitoring with Acoustic Emission (AE) Part I: Signal Characterization and Stock Hardness Effects," *Journal of Engineering Materials and Technology*, vol. 105, no. 4, pp. 295-300, 1983, doi: 10.1115/1.3225661.
- [20] B. S. Kim, "Punch Press Monitoring with Acoustic Emission (AE) Part II: Effects of Process Variables," *Journal of Engineering Materials and Technology*, vol. 105, no. 4, pp. 301-306, 1983, doi: 10.1115/1.3225662.
- [21] J. Song, S. Kim, Z. Liu, N. N. Quang, and F. Bien, "A Real Time Nondestructive Crack Detection System for the Automotive Stamping Process," *IEEE Transactions on Instrumentation and Measurement*, vol. 65, no. 11, pp. 2434-2441, 2016, doi: 10.1109/TIM.2016.2583218.
- [22] S. Rangwala, S. Liang, and D. Dornfeld, "Pattern recognition of acoustic emission signals during punch stretching," *Mechanical Systems and Signal Processing*, vol. 1, no. 4, pp. 321-332, 1987/10/01/ 1987, doi: 10.1016/0888-3270(87)90092-6.
- [23] S. Y. Liang and D. A. Dornfeld, "Characterization of Sheet Metal Forming Using Acoustic Emission," *Journal of Engineering Materials and Technology*, vol. 112, no. 1, pp. 44-51, 1990, doi: 10.1115/1.2903185.
- [24] V. V. Shanbhag, B. F. Rolfe, N. Arunachalam, and M. P. Pereira, "Investigating galling wear behaviour

- in sheet metal stamping using acoustic emissions," *Wear*, vol. 414-415, pp. 31-42, 2018/11/15/ 2018, doi: 10.1016/j.wear.2018.07.003.
- [25] S. Hao, S. Ramalingam, and B. E. Klamecki, "Acoustic emission monitoring of sheet metal forming: characterization of the transducer, the work material and the process," *Journal of Materials Processing Technology*, vol. 101, no. 1, pp. 124-136, 2000/04/14/ 2000, doi: 10.1016/S0924-0136(00)00441-6.
- [26] S. Abdelkrim and C. Hervé, *MONITORING OF STAMPING BY ACOUSTIC EMISSION (AE)*. 2018.
- [27] J. M. Griffin, V. V. Shanbhag, M. P. Pereira, and B. F. Rolfe, "Application of machine learning for acoustic emissions waveform to classify galling wear on sheet metal stamping tools," *The International Journal of Advanced Manufacturing Technology*, vol. 116, no. 1, pp. 579-596, 2021/09/01 2021, doi: 10.1007/s00170-021-07408-5.
- [28] M. Ge, G. Zhang, R. Du, and Y. Xu, "Feature Extraction From Energy Distribution of Stamping Processes Using Wavelet Transform," *Journal of Vibration and Control*, vol. 8, pp. 1023-1032, 07/01 2002, doi: 10.1177/107754602029577.
- [29] D. Y. Sari, T.-L. Wu, and B.-T. Lin, "Preliminary study for online monitoring during the punching process," *The International Journal of Advanced Manufacturing Technology*, vol. 88, no. 5, pp. 2275-2285, 2017/02/01 2017, doi: 10.1007/s00170-016-8956-y.
- [30] G. C. Zhang, M. Ge, H. Tong, Y. Xu, and R. Du, "Bispectral analysis for on-line monitoring of stamping operation," *Engineering Applications of Artificial Intelligence*, vol. 15, no. 1, pp. 97-104, 2002/02/01/ 2002, doi: 10.1016/S0952-1976(02)00007-6.
- [31] C.-Y. Huang and Z. Dzulfikri, "Stamping Monitoring by Using an Adaptive 1D Convolutional Neural Network," *Sensors*, vol. 21, no. 1, doi: 10.3390/s21010262.
- [32] T.-L. Wu, D. Y. Sari, B.-T. Lin, and C.-W. Chang, "Monitoring of punch failure in micro-piercing process based on vibratory signal and logistic regression," *The International Journal of Advanced Manufacturing Technology*, vol. 93, no. 5, pp. 2447-2458, 2017/11/01 2017, doi: 10.1007/s00170-017-0701-7.
- [33] T. Ohashi, "Feature extraction for machine learning to detect floating scrap during stamping using accelerometer," *Journal of Advanced Mechanical Design, Systems, and Manufacturing*, vol. 18, no. 4, pp. JAMDSM0052-JAMDSM0052, 2024, doi: 10.1299/jamdsm.2024jamdsm0052.